CIRP Annals - Manufacturing Technology 72 (2023) 477–480

Contents lists available at ScienceDirect

CIRP Annals - Manufacturing Technology

journal homepage: https://www.editorialmanager.com/CIRP/default.aspx

A process chain for the mass production of nanopatterned bactericidal plastic parts

Marco Sorgato[a], Paola Brun[b], Enrico Savio (1)[a], Giovanni Lucchetta (2)[a,*]

[a] Department of Industrial Engineering, University of Padova, via Venezia 1, Padova, 35131, Italy
[b] Department of Molecular Medicine, University of Padova, via Gabelli 63, Padova, 35121, Italy

ARTICLE INFO

Article history:
Available online 15 April 2023

Keywords:
Nano structure
Replication
Antibacterial

ABSTRACT

Surface nanopatterning of plastic parts is a promising solution to enable the mass production of bactericidal applications without using antibiotics. In this work, an innovative process chain for efficiently manufacturing bactericidal parts was developed and validated. It is based on a particular type of laser-induced periodic surface structuring of injection molds that can be effectively replicated onto size-tunable bactericidal nanopatterns. Their polyvalent bactericidal performance directly correlates with the surface feature parameters *Shh*, *Spd*, and *Spc*, showing that higher, denser, and sharper spikes are more effective in killing bacteria by perforating their membrane.

1. Introduction

Developing new process chains to enable the high-volume manufacture of antibacterial surfaces on plastic parts is crucial to prevent potential threats from bacteria due to the broad application of polymeric materials in industry and medicine. The most efficient current strategies to avoid bacterial-associated infections rely on the local release of antibacterial agents from coatings or drug-impregnated plastic compounds. Critical limitations of these chemistry-based strategies are their limited effectiveness in time, growing concerns about the increasing resistance of bacteria against antibiotics, and the long-term toxicity of metallic nanoparticles and chemical agents on humans.

More recently, mechanical cues such as surface nanopatterns (NP) have been recognized to offer a significant antibacterial effect without the need for antibiotics [1–4]. Their effect can be divided into two categories: (i) antibiofouling surfaces for preventing the initial attachment of bacteria; and (ii) bactericidal surfaces for killing attached bacteria. Antibiofouling surfaces have been extensively investigated as their effect is usually based on the superhydrophobicity obtained by combining low surface energy polymers with rough surfaces [1].

On the other hand, the high-volume manufacture of bactericidal surfaces at different length scales with high reproducibility is still challenging, as it relies on the replication of nanoholes onto high aspect ratio nanostructures, which can stretch the bacteria's cell membrane when in close contact [2]. There is not yet total agreement on the complex bactericidal mechanism. While bacterial death on contact with NPs is often attributed to membrane rupture by perforation [3], recent studies have shown that physical stress due to membrane stretching, without an immediate break, leads to increased bacterial death [4].

The bactericidal mechanism is further complicated by the different characteristics of various bacteria, which exhibit diverse responses to the shape and dimensions of NPs. Bacteria come in multiple forms but are typically only a few micrometers long. They have been broadly divided into Gram-negative and Gram-positive groups based on the structural properties of their cell walls. The first group is typically distinguished by a relatively thin layer between the cytoplasmic and outer membranes, whereas the latter has a significantly thicker cell wall. Therefore, the bactericidal activity of nanopillars is stronger for cells of Gram-negative bacteria, such as *Escherichia coli* and *Pseudomonas aeruginosa* (Fig. 1a). Instead, highly sharp NPs are often reported to be more effective against Gram-positive bacteria (e.g. *Staphylococcus aureus*) [5].

In polyvalent bactericidal surfaces, NP spacing should be smaller than the size of the bacteria to prevent bacterial adhesion in the valleys (Fig. 1b). However, if the nanostructures are too dense, they inhibit the bacterial wall from stretching [6]. Furthermore, the level of bactericidal behavior correlates with the degree of bacterial adhesion, which in turn is governed by nanostructures diameter [7]. Theoretical studies on nanopillars showed that a large radius increases the stretching degree. Furthermore, if the radius is smaller than a critical value, a bacterial cell cannot adhere and be stretched [8].

Although most effective bactericidal NPs described in the literature have dimensions of 100–500 nm in height, 10–300 nm in diameter, and 380–1080 nm in spacing, their optimum shape and sizes still need to be identified [6]. Moreover, such NPs need to be replicated on plastic parts through scalable industrial processes directly applicable for commercial use, such as injection molding. A wide range of patterning techniques, such as nanoimprint lithography and a combination of colloidal lithography and plasma etching, have been developed to produce a variety of micro-nanopatterned polymer topographies [9–11].

* Corresponding author.
E-mail address: giovanni.lucchetta@unipd.it (G. Lucchetta).

https://doi.org/10.1016/j.cirp.2023.04.014

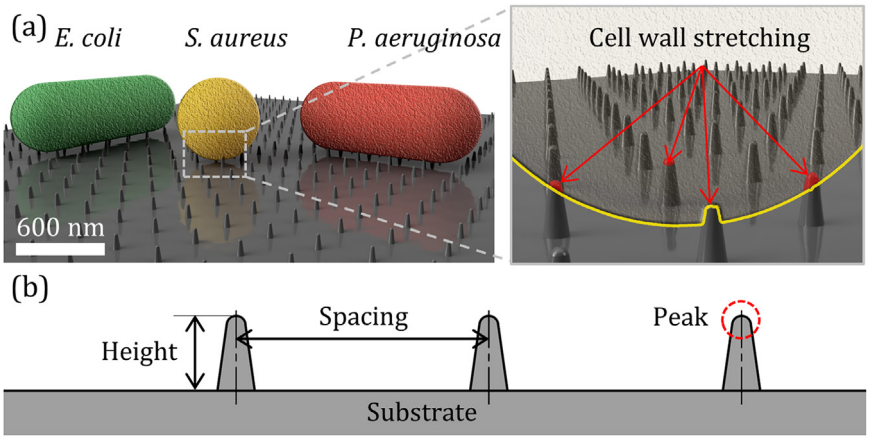

Fig. 1. (a) Schematic illustration of the NPs bactericidal mechanism. (b) Description of the NPs main geometrical parameters.

However, such nanopatterning techniques cannot be applied to industrial injection molding. Therefore, this paper proposes an innovative process chain based on a particular type of laser-induced periodic surface structuring (LIPSS) that combines low spatial frequency LIPSS (LSFL) and high spatial frequency LIPSS (HSFL) to fabricate a ladder-like texture on a mold cavity surface [12]. The size and shape of the nanoholes formed between the ladder rungs and rails were varied using the texturing parameters to obtain three different NPs to be replicated on plastic samples. Their bactericidal performance was then tested and related to the areal surface texture parameters, including the feature parameters defined by ISO 25,178−2:2022.

2. Materials and methods

2.1. Bactericidal surface fabrication

The molded samples were designed as 7.5 mm diameter and 2 mm thickness disks, having the nanopatterns replicated only on one face. The mold cavity was side gated using a cold runner, as shown in Fig. 2. The polymer used for the samples is commercial polypropylene (PP), which is widely used in automotive and home appliance applications and has no bactericidal effect. A modular mold assembly was used to mount inserts with different nanopatterns.

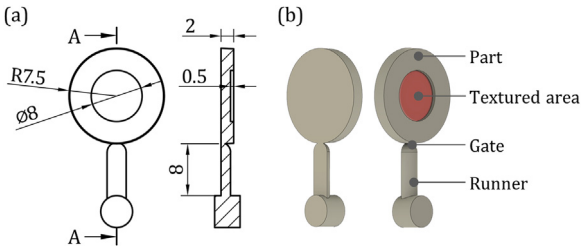

Fig. 2. Molded samples (a) design and (b) location of the textured area (dimensions in millimeters).

The injection mold inserts were made of 16MnCr5 steel and polished to obtain a surface roughness of $Sa < 0.03$ μm applying a form removal by subtraction of least squares mean plane and filters λ_s=2.5 μm and λ_c=0.8 mm.

A picosecond laser (EKSPLA, Atlantic 50-IR-GR25-UV18), with a pulse duration of about 10 ps, was used to create three different nanopatterns on the mold inserts. Beamlines with wavelengths λ=1064 nm and λ=532 nm were used. The inserts were textured using two Raylase Superscan V scanning heads with an input aperture of 14 mm and equipped with 80 and 75 mm focal length F-theta lenses. Both the beamlines are characterized by a focalized $1/e^2$ beam diameter of about 10 µm. Table 1 summarizes the parameters of the three different texturing conditions. Scanning speed and repetition rate guarantee a homogeneous distribution of pulses with a pitch of 3 and 4 µm for the first and second harmonic, respectively.

Table 1
Laser parameters for the texturing of the mold inserts.

Mold texture	Wavelength / nm	Power / mW	# Passes	Repetition rate /kHz	Speed / mm/s
LIPSS 1	532	46	1	400	1200
LIPSS 2	532	27	3	400	1200
LIPSS 3	1064	242	1	400	1600

A micro injection molding machine (Wittmann Battenfeld, MicroPower 15) was used to replicate the nanopatterns on polypropylene samples. The rapid heat cycle molding technology was used to maximize the replication of the nanopatterns [13]: before the injection phase, the mold was heated up to 100 °C, and after the cavity was filled, it was quickly cooled to 40 °C. The injection flow rate (Q = 3.75 cm^3/s) and the holding pressure (pH=700 bar) were set to values achievable using a conventional injection molding machine to prove that the proposed process chain is suitable for large-scale manufacturing.

2.2. Surface characterization

The textured inserts were first inspected from a qualitative point of view using a scanning electron microscope (SEM) to ascertain the presence of periodic structures by using a magnification up to 30,000 × . The nanopatterns were characterized by confocal microscopy (Sensofar Neox) on both the mold and the replicated surfaces, using a 100 × magnification objective with spatial sampling of 140 nm and vertical resolution of 2 nm.

The acquired height maps with lateral dimensions of 120 × 120 μm^2 were subjected to form removal by subtraction of the mean plane. Three repeated acquisitions of each texture were performed for both the mold and the plastic parts to compute the surface texture parameters on the S-L surface according to ISO 25,178−2:2022, with an L-filter equal to 2.5 μm.

Since peaks are recognized as the most bactericidal surface features, watershed segmentation with a wolf pruning equal to 5% of *Sz* was applied to the topographic maps. This method allows the automatic identification and characterization of significant peaks on hills (for the replicated samples) and pits on dales (for the textured molds). Surface topography measurements were analyzed in terms of arithmetic mean height, *Sa*, and areal texture feature parameters: mean hills height, *Shh*, mean dales depth, *Sdd*, the density of peaks, *Spd*, and arithmetic mean peak curvature, *Spc*.

As the presence of the NPs may affect the surface wettability of the plastic samples and thus the bacterial cell retention, the static water contact angle, θ, was assessed for all the samples using the sessile drop method with a water droplet volume of 15 μL.

2.3. Evaluation of bactericidal activities

Staphylococcus aureus (strain designation NCTC 8530), *Pseudomonas aeruginosa* (strain designation 109,246), and *E. coli* (strain

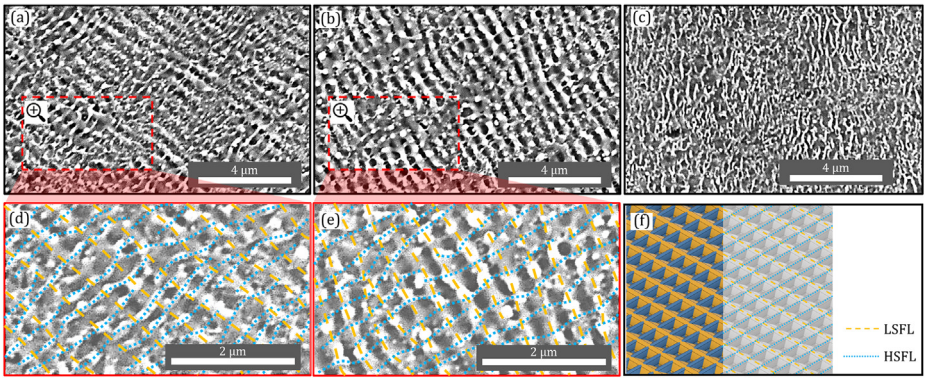

Fig. 3. SEM images of the laser-ablated mold textures for (a) LIPSS 1, (b) 2, and (c) 3. Ladder-like structure evidenced on (d) LIPSS 1 and (e) 2. Schematic of the (f) ladder-like pattern.

designation HB101) were purchased from ATCC (LGC Standards, Milan, Italy) and cultured on Trypticase soy broth (*S. aureus* and *P. aeruginosa*) or lysogeny broth (*E. coli*), all provided by Fisher Scientific. At the time of the experiments, fresh inocula were grown for 16 h at 37 °C under agitation (150 rpm). At the end of incubation, the concentration of the bacterial cultures was adjusted to 0.5 McFarland (1.5×10^8 colony forming units, CFU/ml).

The molded samples were decontaminated by incubation for 10 min in ethanol 70% vol/vol and subsequent ethanol evaporation under sterile conditions for 16 h. Bacterial cultures were centrifuged, suspended in growth media to obtain 1×10^4 CFU, and then seeded on the samples at 37 °C for 30 min to 48 h. Culture plates were positioned in a humidification chamber for longer incubation times to prevent medium evaporation. At the end of incubation, 1 ml of fresh medium was added to the surfaces of the plastic samples and vortexed for 5 min to detach all bacterial cells. The samples were then transferred in a new sterile tube, diluted adequately in culture media, and cultured on agar plates. Plates were incubated at 37 °C for 16 h. Bacterial colonies were counted. Bactericidal results are reported as the percentage of dead cells relative to bacterial cultures seeded on control surfaces (molded using unpatterned inserts) and evaluated at every time point as described above.

3. Results and discussion

3.1. Surface nanopatterning

As shown in Fig. 3a and 3b, the mold textures LIPSS 1 and 2 are characterized by a ladder-like pattern formed by LSFL and HSFL. The schematic of this pattern is shown in Fig. 3f and superimposed to the LIPSS in Fig. 3d and 3e. LSFL are ripples with higher periodicity oriented perpendicular to the incident polarization, while HSFL are lower periodic structures parallel to the incident polarization [12]. The formation of the HSFL embedded inside the LSFL is challenging and can only be observed using low pulse numbers (LIPSS 1) or laser fluences (LIPSS 2) [14]. HSFL are distorted or destroyed at either higher or lower energies. The better regularity and definition of the LIPSS 2 texture were obtained by decreasing the energy per pulse and increasing the pulse number. In the LIPSS 3 texture, only HSFL can be observed because the low values used for both laser pulse number and fluence prevent the LSFL from appearing [14].

Table 2
Surface characterization results for mold textures (M) and NPs replicated on plastic samples (S) – standard deviations in brackets.

Parameter	Control	LIPSS 1	LIPSS 2	LIPSS 3
Sa (M) /nm	426 (12)	26 (5)	21 (3)	15 (4)
Sa (S) /nm	408 (16)	22 (4)	19 (5)	12 (5)
Sdd (M) /nm	63 (4)	13 (2)	19 (2)	10 (3)
Shh (S) /nm	61 (3)	15 (3)	21 (3)	9 (2)
Spd (S) /μm^{-2}	–	0.098 (0.02)	0.168 (0.03)	0.118 (0.02)
Spc (S) /μm^{-1}	–	0.179 (0.04)	0.354 (0.05)	0.122 (0.03)
θ (S) /°	78 (2)	108 (2)	121 (2)	104 (2)

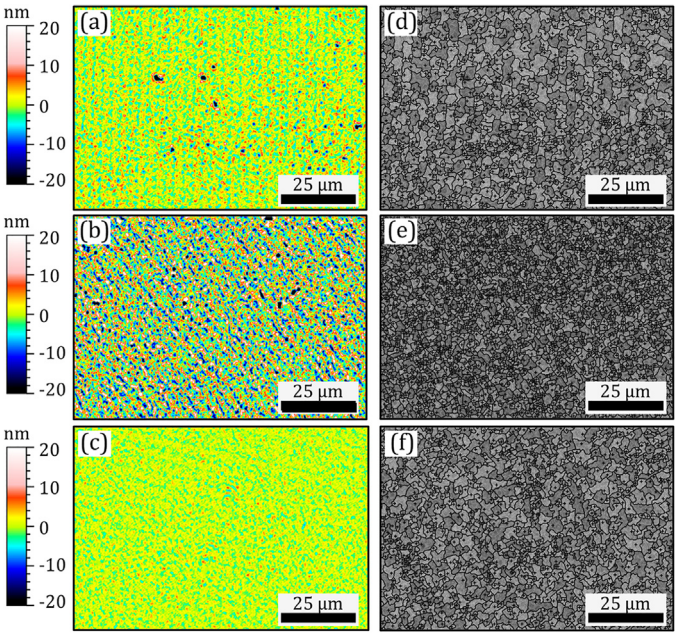

Fig. 4. Height maps of the replicated NPs for (a) LIPSS 1, (b) 2 and (c) 3, and (d-f) their corresponding segmented results.

The increased periodicity of the HSFL is due to the higher wavelength of the beamline. The surface characterization results (Table 2) show that the injection molding process effectively replicates the mold inserts: the *Sa* values of the replicated topographies are comparable to the ones of the related mold textures. Nanoholes in the mold textures were replicated onto peaks in the corresponding polymer NPs resulting in *Sdd* values for the mold very close to the *Shh* results for the samples. The height maps and the segmented results shown in Fig. 4 reveal that the ladder-like textures were replicated onto spike-like patterns characterized by different values of height and spacing. LIPSS 1 and 3 have a similar density of peaks (Fig. 4d and 4f), but the height is lower for the latter. LIPSS 2 shows the highest peak height and density (Fig. 4b and 4e).

Therefore, the proposed process chain proves suitable for controlling the NPs characteristics that govern the bactericidal effect (i.e. height and spacing) by varying the laser texturing parameters. While the control sample surface is hydrophilic (with a contact angle of 78° reported in Table 2), all the LIPSS NPs are hydrophobic. In particular, LIPSS 2 has a larger wettability, with a contact angle of 121°, due to its higher and denser peaks.

3.2. Bactericidal performance

As shown in Fig. 5, the NPs bactericidal performance is significant on all the species, proving that the obtained NPs are polyvalent. The general trend shows a high bactericidal action within the first 30 min of contact (~60%), which further increases (~90%) after 24 h. LIPSS 2 generally performs better, and this can be due to its higher and closer

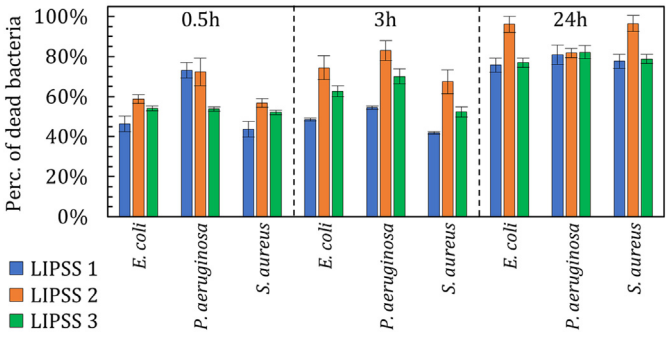

Fig. 5. Bactericidal performance evolution of the tested NPs compared to the control surface.

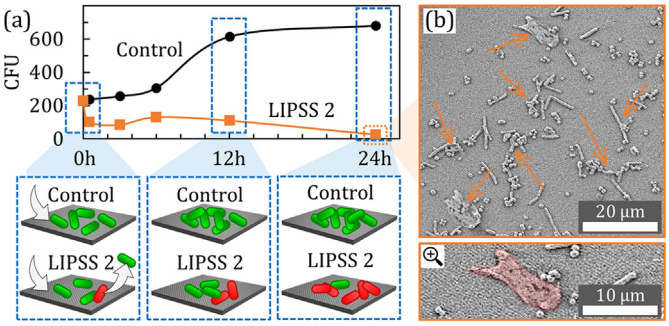

Fig. 6. (a) Bacterial growth curve for the LIPSS 2 and the control surfaces; (b) rupturing of the bacterial cell wall by LIPSS 2 NPs.

peaks. The bacterial growth curve shown in Fig. 6a represents the number of *S. aureus* live cells on the LIPSS 2 and the control surfaces over the observation time.

The curve of the control surface has three typical distinct phases: lag, exponential, and stationary. In the lag phase (first 6 h), bacteria are metabolically active but not dividing. The exponential growth lasts 6 h and ends when the curve reaches a plateau (after 12 h) as the number of dying cells equals the number of dividing cells. On the contrary, the number of bacterial cells seeded on the LIPSS 2 samples initially decreases due to both the bactericidal effect reported in Fig. 5 and the marked hydrophobicity of the surface, which affects the initial bacterial retention. After 6 h, the curve of the LIPSS 2 sample does not show an exponential growth but just a slight increase due to the significant bactericidal activity of the NP (Fig. 6b), which counteracts the bacteria proliferation and eventually overcomes it. In fact, from 12 to 24 h, the curve slowly but steadily decays as the number of dying cells exceeds the number of dividing cells.

Three interesting correlations were identified between the bactericidal performance of the NPs (averaged among the three tested bacteria at 24 h) and the corresponding surface feature parameters, as reported in Fig. 7. The percentage of dead bacteria is directly correlated with *Shh* ($r = 0.83$) and *Spd* ($r = 0.98$), as shown in Fig. 7a and 7b, respectively. As explained in Section 1, higher and closer peaks have a more significant bactericidal activity due to the increased stretching of the bacterial wall. Fig. 7c shows the direct correlation ($r = 0.95$) with the mean peak curvature, *Spc*. The evidence that sharper peaks increase bacterial death supports the original theory that identifies membrane rupture by perforation (Fig. 6b) as the prevalent bactericidal mechanism [3].

4. Conclusion

The process chain proposed in this work consists of nanopatterning an injection mold cavity with a combination of low and high-spatial frequency LIPSS to fabricate a ladder-like texture that can be replicated on plastic parts for the high-volume manufacture of bactericidal surfaces without using antibiotics. The NPs characteristics that govern the bactericidal effect were

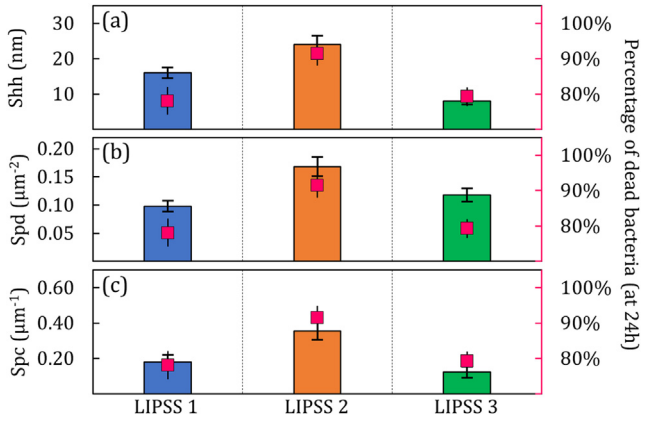

Fig. 7. Average bactericidal performance of the tested NPs (points) compared with the most influential surface feature parameters (bars) identified as the spikes' height, spacing, and sharpness.

Larger, denser, and sharper spikes are more efficient at killing bacteria by perforating their membrane. In the proposed process chain, these feature parameters can be optimized by varying the laser texturing wavelength, the energy per pulse, and the pulse number. Given the weakness of the polymer nanostructures, this solution is particularly indicated for out-of-reach surfaces that cannot be easily sanitized but are critical for bacteria proliferation, such as automotive air ducts and residential ventilation systems. The antibacterial performance is expected to be maintained as long as the airflow keeps the surface clean.

Declaration of Competing Interest

The authors declare that they have no known competing financial interests or personal relationships that could have appeared to influence the work reported in this paper. Project funded under the UniImpresa 2021 program sponsored by the University of Padova

References

[1] Francone A, Merino S, Retolaza A, Ramiro J, Alves SA, de Castro JV, Neves NM, Arana A, Marimon JM, Torres CMS, Kehagias N (2021) Impact of surface topography on the bacterial attachment to micro- and nano-patterned polymer films. *Surfaces and Interfaces* 27:101494.
[2] Linklater DP, Baulin VA, Juodkazis S, Crawford RJ, Stoodley P, Ivanova EP (2021) Mechano-bactericidal actions of nanostructured surfaces. *Nature Reviews Microbiology* 19/1:8–22.
[3] Tripathy A, Sen P, Su B, Briscoe WH (2017) Natural and bioinspired nanostructured bactericidal surfaces. *Advances in Colloid and Interface Science* 248:85–104.
[4] Li X (2016) Bactericidal mechanism of nanopatterned surfaces. *Physical Chemistry Chemical Physics* 18/2:1311–1316.
[5] Maleki E, Mirzaali MJ, Guagliano M, Bagherifard S (2021) Analyzing the mechano-bactericidal effect of nano-patterned surfaces on different bacteria species. *Surface and Coatings Technology* 408:126782.
[6] Modaresifar K, Azizian S, Ganjian M, Fratila-Apachitei LE, Zadpoor AA (2019) Bactericidal effects of nanopatterns: A systematic review. *Acta Biomaterialia* 83:29–36.
[7] Nowlin K, Boseman A, Covell A, LaJeunesse D (2015) Adhesion-dependent rupturing of Saccharomyces cerevisiae on biological antimicrobial nanostructured surfaces. *Journal of The Royal Society Interface* 12/102.
[8] Li X, Chen T (2016) Enhancement and suppression effects of a nanopatterned surface on bacterial adhesion. *Physical Review E* 93/5:052419.
[9] Echeverria C, Torres MDT, Fernández-García M, de la Fuente-Nunez C, Muñoz-Bonilla A (2020) Physical methods for controlling bacterial colonization on polymer surfaces. *Biotechnology Advances* 43:107586.
[10] Mo S, Mehrjou B, Tang K, Wang H, Huo K, Qasim AM, Wang G, Chu PK (2020) Dimensional-dependent antibacterial behavior on bioactive micro/nano polyetheretherketone (PEEK) arrays. *Chemical Engineering Journal* 392:123736.
[11] Linklater DP, Saita S, Murata T, Yanagishita T, Dekiwadia C, Crawford RJ, Masuda H, Kusaka H, Ivanova EP (2022) Nanopillar Polymer Films as Antibacterial Packaging Materials. *ACS Applied Nano Materials* 5/2:2578–2591.
[12] Taher MA, Chaudhary N, Thirunaukkarasu K, Rajput VK, Naraharisetty SRG (2022) Controlled periodicities of ladder-like structures via femtosecond laser of wavelength from 400nm to 2200nm. *Surfaces and Interfaces* 28:101622.
[13] Sorgato M, Guidi E, Conconi MT, Lucchetta G (2021) Surface nanostructuring of bioresorbable implants to induce osteogenic differentiation of human mesenchymal stromal cells. *CIRP Annals* 70/1:463–466.
[14] Liu K, Li X, Xie C, Wang K, Zhou Q, Qiu R (2017) Formation of sub-200nm nanostructure on Fe film irradiated by femtosecond laser. *Optics & Laser Technology* 94:28–33.